Received 28 August 2023; revised 5 October 2023; accepted 9 October 2023. Date of publication 17 October 2023; date of current version 10 November 2023.

Digital Object Identifier 10.1109/OJAP.2023.3325055

2×2 Lens Array Antenna Using Square-Bottom Concave-Convex Lens in 300-GHz Band

BAZILAH BAHAROM[1] (Graduate Student Member, IEEE), YOSHIKI SUGIMOTO[1] (Member, IEEE), BAKAR ROHANI[1] (Member, IEEE), KUNIO SAKAKIBARA[1] (Senior Member, IEEE), NOBUYOSHI KIKUMA[1] (Senior Member, IEEE), YOSHIHIDE YAMADA[2] (Senior Member, IEEE), AND NURUL HUDA ABD RAHMAN[3] (Member, IEEE)

[1]Department of Electrical and Mechanical Engineering, Nagoya Institute of Technology, Nagoya 466-8555, Japan
[2]Malaysia Japan International Institute of Technology, Universiti Teknologi Malaysia, Kuala Lumpur 54100, Malaysia
[3]Antenna Research Center, School of Electrical Engineering, College of Engineering, Universiti Teknologi MARA, Shah Alam 40450, Malaysia

CORRESPONDING AUTHOR: Y. SUGIMOTO (e-mail: sugimoto.yoshiki@nitech.ac.jp)

This work was supported in part by the Ministry of Internal Affairs and Communications of Japan with a Scheme of Research and Development for Expansion of Radio Wave Resources under Grant JPJ000254, and in part by the Commissioned Research by the National Institute of Information and Communications Technology (NICT), Japan, under Grant 00401.

ABSTRACT A 2 × 2 lens array provides a half reduction of antenna height compared to the twice-diameter single-feed lens antenna with an almost similar gain performance due to the same aperture size. However, it generally suffers from a non-uniform amplitude distribution of each lens, which degrades the overall lens antenna performance. This study proposes a 2 × 2 lens array antenna composed of square-bottom lenses with a concave-convex lens shaping design to improve the uniformity and aperture efficiency. The measured results of the proposed 2 × 2 square-bottom concave-convex lens array antenna with a lens height of 9.74 mm achieved a boresight gain of 34.9 dBi, and the lowest sidelobe level observed was greater than −12 dB in the 300-GHz band.

INDEX TERMS Lens antenna, concave-convex, antenna array, sub-terahertz.

I. INTRODUCTION

MILLIMETER-WAVE (mm-wave) and terahertz-wave (THz-wave) wireless communication systems are in increasing demand owing to their large data capacity and low latency. These wireless communication systems face increasing requirements for higher data rates and more simultaneous users [1]. Recently, the planning and visioning of possible solutions for the beyond 5G (5th generation mobile communication systems) and the 6G (6th generation mobile communication systems) for short-distance and high data rates in wireless communications have already begun [2]. Thus, owing to the fast development in electronic device systems, the required applications of mm-waves and THz-waves have increased rapidly in terms of high-definition (HD) digital video and related multimedia entertainment services [3], [4], [5]. Moreover, requirements for sensing applications such as radar, remote sensing, radio astronomy, imaging sensing for medical applications, radiometer systems for space-borne applications, weaponry and contraband detection have also actively increased [6], [7], [8].

Low-profile and compact high-gain antennas are required for THz-wave applications to compensate for sizable atmospheric attenuation [9], [10]. Recently developed antennas operating in the 300-GHz band include a slotted waveguide antenna [11], an integrated LTCC antenna [12], and a corrugated horn antenna [13].

Dielectric lens antennas have also become viable candidates for the 300-GHz band owing to their simple configurations, high gain, and low loss. Recently, lens antennas have been reported operating at 300-GHz bands with various techniques and applications [14], [15], [16], [17], [18], [19], [20]. Dielectric lens antennas also offer a strongly built structure, making them attractive for implementation in communication systems applications. However, a general single-lens antenna has an unavoidable drawback of the high profile entirely due to the focal length and lens thickness. In

addition, recent applications require low-profile and compact antennas. Thus, lens array antennas have been used to overcome these issues.

Lens array antennas have been actively studied over the years. Researchers have proposed many high-performance designs and methods to improve antenna efficiency and achieve high gain throughout all frequency bands. Nevertheless, the implementation of the lens array antenna in mm-waves and THz-waves remains a more significant challenge because of the requirement of special lens shaping design, complex feeding networks, and variations of lens arrangements that cause loss increasing and degrading radiation patterns. Moreover, in THz applications, high-gain antennas with narrow beamwidth and high efficiencies are highly required to improve the signal-to-noise ratio and compensate for the losses of the overall system.

An extended hemispherical lens with a leaky wave feed was proposed to achieve a high aperture efficiency wideband in a tight space design [21]. The gain was 28.7 dBi with an aperture efficiency greater than 60% for a wide bandwidth from 8 to 20 GHz. A half-sphere lens was used to increase the gain of the microstrip from 4.7 to 16.9 dBi with a total average efficiency of approximately 88% [22]. Subsequently, four dielectric hemi-elliptical lens arrays were proposed to achieve a low profile with no performance degradation at 71-76 GHz and 81- 86 GHz [23]. However, all the performance effects of the lens shape used for the lens array above are not discussed thoroughly of how it was developed. Moreover, the lens array design improved the uniform distribution of the lens by shaping the lens surface considering the amplitude distribution [24]; however, the gap space between the circular lens array caused the aperture efficiency to not be fully utilized.

In addition, mm-wave applications require a high-gain lens array with beam-scanning. The combination of beam-scanning of mechanical lens shifting and phased array realizes high-gain beam-scanning [25], [26], [27]. Elliptical lenses are used to achieve high-aperture efficiencies [25], [26]. The boresight peak gains achieved were 27 dBi and 30 dBi with an aperture efficiency of 75% and produced a side-lobe level (SLL) lower than –10 dB at 28 GHz and the W-band, respectively. The scan angles were capable up to ±10° and ±20°. A sparse arrangement of lenses with mechanical displacement relative to their feed provides scanning angles up to ±20° with gain scan loss lower than 2 dB at 550 GHz [27]. To prevent mechanical scanning, electrical antenna switching can be used to achieve a beam-scanning lens array [28]. Lens antenna subarrays using an extended hemispherical lens are developed at 38 GHz, resulting in a maximum gain of 20 dB, with a scanning angle of ±36° and SLL remaining lower than –9.5 dB.

To obtain the maximum gain and the highest aperture efficiency, a lens with a uniform aperture distribution is required. Following the works of [23] and [24], in this paper, a square bottom lens with concave-convex shape which realize uniform amplitude and phase distributions in square aperture is proposed. The proposed lens is suitable for a rectangular arranged lens array. We demonstrate the effectiveness of the proposed lens antenna through electromagnetic simulations and experiments of fabricated antennas.

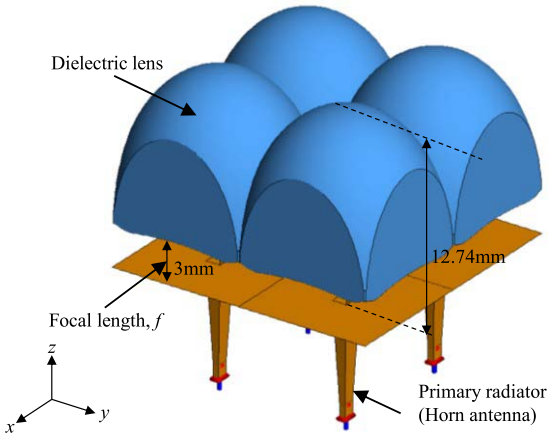

FIGURE 1. 2 × 2 square-bottom concave-convex (Sq-CC) lens array antenna.

The remainder of this paper is organized as follows. Section II introduces the antenna geometry and theory, following the concept of a square-bottom 2 × 2 lens antenna array structure and lens surface shaping using a concave-convex lens. Section III discusses the simulated comparison performance of all single-lens antenna elements. Section IV discusses the simulated comparison performance for all the lens antenna arrays. Measurement validity is presented in Section V. Finally, the conclusions are summarized in Section VI.

II. GEOMETRY AND THEORY

We describe the overall configuration of a 2 × 2 lens array and the design method for the lens elements constituting the array. To investigate the antenna performance, all the lenses were operated with equal parameters, such as material permittivity, focal length, and diameter in the 300 GHz band.

A. PRINCIPLE OF A 2×2 LENS ARRAY

A lens array consists of multiple antenna elements. In this study, it consisted of 2 × 2 lens antennas, each fed by a pyramidal horn antenna. Fig. 1 shows the proposed 2 × 2 square-bottom concave-convex (Sq-CC) lens array antenna. We used a pyramid horn antenna to easily control the beamwidth by changing the horn aperture size. The horn antenna was made of gold-plated copper and fed by a WR-3 standard waveguide. Polypropylene with a dielectric constant, $\varepsilon_r = 2.4$, and dielectric dissipation factor, $\tan\delta = 0.001$ was used as the lens material. It is a readily available, low-loss, machinable plastic that can be manufactured by injection molding for low-cost mass production. It is suitable for mm-wave and THz-wave lens antenna applications [15], [16].

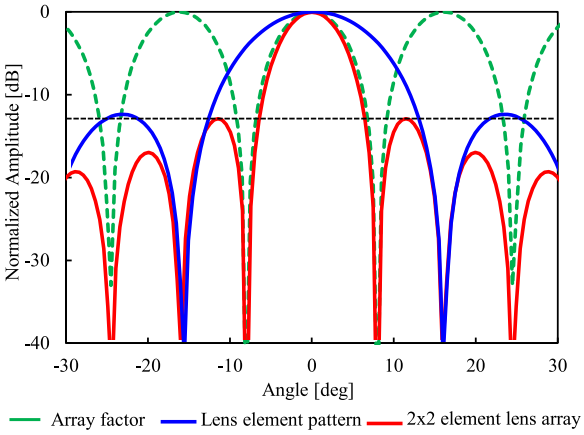

FIGURE 2. Principle equivalence of the lens array with a single lens.

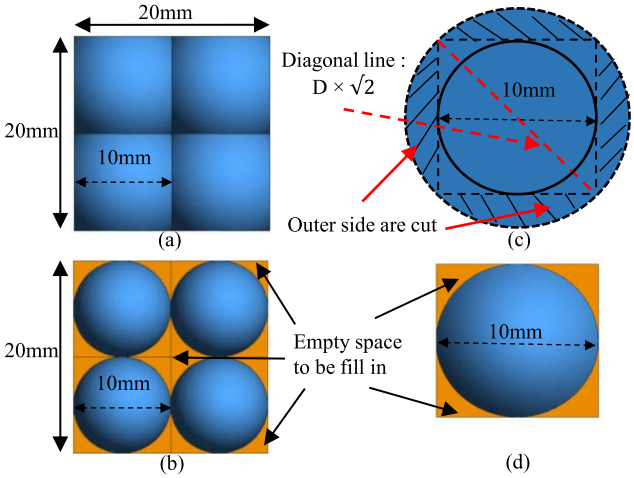

FIGURE 3. Top view schematic of the proposed 2 × 2 lens array antenna with its design parameters: (a) square-bottom lens array, (b) conventional circular lens array, (c) square-bottom single lens, and (d) circular single lens.

Fig. 2 shows the normalized amplitude radiation pattern based on the principal equivalence of a 2 × 2 lens array with a single lens element under a perfectly uniform distribution condition. The diameter of each single lens is 10 λ where λ is a wavelength in free space at 300 GHz. In the 2 × 2 lens array, the total aperture size is 20 λ square. The center spacing between the two lens elements is 10 λ. As the distance between the two lenses is much larger than the wavelength, thus many grating lobes appear within the visible region of the array factor. The lens array radiation pattern can be calculated by simply multiplying the array factor with the single lens pattern. The grating lobes in the array factor are cancelled by the nulls of the single lens element. This happens only when the single lens element pattern provides a uniform distribution condition. The SLL value for uniform amplitude distribution is approximately −13 dB [29]. To satisfy these conditions, the single lens element pattern should have characteristics such as high aperture efficiency and narrow beamwidth and should be as close to a uniform distribution as possible. When all these conditions are satisfied, it suppresses the first SLL to be lower.

However, it is generally difficult to make the aperture distribution of a lens antenna completely uniform. Therefore, in this study, we constructed a lens that improves the uniformity of the aperture distribution and increases the antenna efficiency for a 2 × 2 lens array by using square-bottom and concave-convex lens shapes, as described in the next sub-sections.

B. EXTENSION TECHNIQUES OF LENS APERTURE (SQUARE-BOTTOM)

An extension technique of the lens aperture using a square-bottom lens profile is proposed to utilize the antenna plane effectively and to achieve a higher gain. Fig. 3 shows the geometry comparison of the lens profiles of the circular and square bottom lenses. Four circular lens antennas were placed in a rectangular arrangement to form the 2 × 2 lens array, with vacant spaces at each corner of the circular lenses as shown in Fig. 3. (b). In addition, a gap appears in the middle of the square arrangement, decreasing the aperture efficiency, thus, the entire antenna aperture cannot be used efficiently. To address this, we proposed a square bottom lens array to fill the space and increase the aperture efficiency of the rectangular array, as shown in Fig. 3 (a). The diameter of the circular lens is 10 mm, as shown in Fig. 3 (d). In designing the shape of the square-bottom lens, the total lens diameter corresponds to the diagonal length of the square. Subsequently, the outer four sides of the square were cut to realize a square-bottom lens, as shown in Fig. 3 (c). The physical aperture area of the square-bottom lens is $4/\pi$ larger than that of the circular lens. An improvement in the effective aperture efficiency can be expected when a rectangular array is constructed using a square bottom lens.

C. LENS SURFACE SHAPING TECHNIQUE (CONCAVE-CONVEX)

Lens shaping has been extensively studied for various applications of dielectric lenses [30], [31], [32], [33], [34]. One of the simplest plano-convex (PC) lens is known for controlling only the aperture phase distributions. The lens shape has a flat surface on the inner side and a curved surface on the outer side [30], [33]. Because the PC lens does not have an adjustment parameter to control the amplitude distribution, the aperture distribution corresponds to the radiation pattern of the primary radiator; therefore, the aperture efficiency is low. A concave-convex (CC) lens is proposed to control both the amplitude and phase distributions. Concave-convex lens form curved surfaces on their outer and inner surfaces, which control both the aperture amplitude and phase distributions. This lens is known for its high directivity and providing more uniform amplitude distribution [31].

The geometrical concept of the CC lens shaping design is illustrated in Fig. 4. The design was based on the

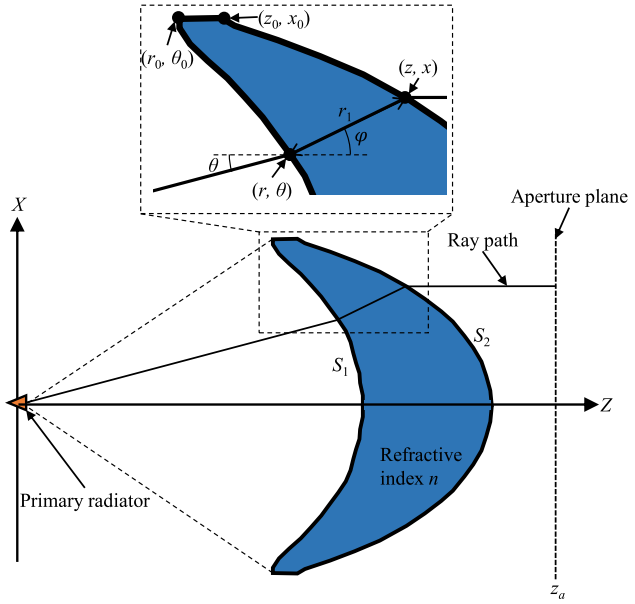

FIGURE 4. Geometrical concept of the concave-convex lens shaping.

spherical or elliptical lens condition conceived by the authors of [31], [32], [33]. This section describes the design method to validate the proposed lens surface design. The lens is designed based on the surface curves of the inner side ($S_1(r, \theta)$) and outer side ($S_2(z, x)$). An optical ray approximates an electromagnetic (EM) wave radiated from a primary radiator. The lens diameter was selected based on the required gain. The basis lens surface design is achieved using the following three essential equations based on the fundamental ray equation developed from Snell's law. The (S_1) side is derived as in equation (1):

$$\frac{dr}{d\theta} = \frac{nr\ \sin(\theta - \varphi)}{n\ \cos(\theta - \varphi) - 1} \tag{1}$$

The (S_2) side is derived as in equation (2), where n is the refractive index corresponding to $\sqrt{\varepsilon_r}$, and φ is the refracted angle of the lens. The expressions for the condition that the ray exits parallel to the z-axis after refraction in the lens can be derived for the (S_2) surface as:

$$\frac{dz}{dx} = \frac{n\ \sin(\varphi)}{1 - n\ \cos(\varphi)} \quad \frac{dz}{d\theta} = \frac{n\ \sin(\varphi)}{1 - n\ \cos(\varphi)} \frac{dx}{d\theta} \tag{2}$$

The aperture plane is arbitrarily defined to be sufficiently far from the primary radiator for the convenience to measure the length of the ray path through the lens. The condition of the total electric path length, L_t to be constant is derived as:

$$L_t = r + nr_1 + z_a\ - z \tag{3}$$

$$r_1 = \frac{z\ -\ r\ \cos\ (\theta)}{\cos(\varphi)} \tag{4}$$

where z_a indicates the position of the aperture plane. The radiation pattern $E_p(\theta)$ of the primary radiator and the aperture distribution $E_d(x)$ are important parameters in the design of a CC lens. Therefore, we relate the given pattern to the required $E_p(\theta)$ to the required aperture distribution $E_d(x)$ through the following electric power conservation condition in differential system equations as follows:

$$\frac{dx}{d\theta} = \frac{E_p^2(\theta)}{P} \frac{D}{E_d^2(x)} \tag{5}$$

where the total power of the primary radiator, P is derived as,

$$P = \int E_p^2(\theta)\ d\theta \tag{6}$$

and, the total power D, on the aperture plane, is derived as follows:

$$D = \int E_d^2(x)\ dx \tag{7}$$

The radiation pattern of the primary radiator can be approximately expressed using the directive parameter m as:

$$E_p^2(\theta) = \cos\ ^m\theta \tag{8}$$

We derived the parameter m in (8) to fit the actual beamwidth of the primary radiator. The constant value C indicates the center-to-edge ratio of the amplitude distribution over the aperture plane. The power distribution $E_d^2(x)$ over the aperture can be approximated by C as:

$$E_d^2(X) = \left[1 - \left(1 - \frac{1}{C}\right)\left(\frac{x}{x_0}\right)\right]^p \tag{9}$$

For the initial values, the coordinates at the lens edge are arbitrarily determined as (k_0, θ_0) and (z_0, x_0). The lens projection angle θ_0 is the angle between the lens axis toward the lens edge. By solving the system of the differential equations with $\frac{dr}{d\theta}$, $\frac{dz}{d\theta}$, and $\frac{dx}{d\theta}$ given by (1), (2), and (5), respectively, the surface shape of the lens is obtained from $\theta = 0$ to θ_0. In this study, we designed a uniform aperture distribution where, C is set to 1.

The focal length to diameter (F/D) ratio used in this work was 0.3. When the focal length was small, the lens thickness increased for a uniform phase distribution. F/D was chosen to balance between the height of the focal length and lens thickness to achieve a low-profile lens antenna. When F/D is chosen to be 0.3, the lens projection angle θ_0 is calculated at 59 degrees. Controlling the beamwidth of the horn antenna as a primary radiator provides adequate illumination that collimates toward the lens and minimizes the spillover and illumination loss [35], [36]. Further investigation of the lens edge level is presented in Section III. To demonstrate the effectiveness of the proposed antenna, we compared the performances of the concave-convex square-bottom lens with the simple circular-bottom plano-convex lens.

III. SIMULATION PERFORMANCE OF SINGLE LENS

This section compares the simulation results of all four types of single-lens elements in the 300 GHz band using the EM simulation software FEKO. The main factors used to evaluate the antenna performance are the reflection

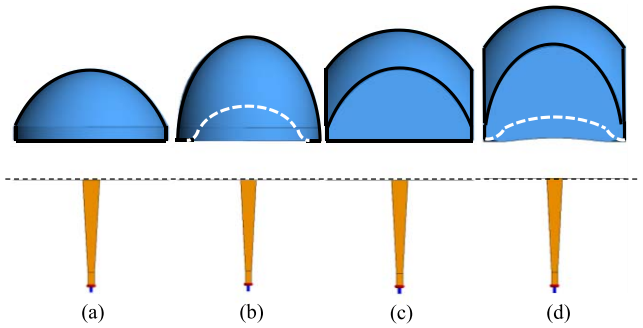

FIGURE 5. Sideview of the lens antenna shape (a) Cr-PC lens (b) Cr-CC lens (c) Sq-PC lens, and (d) Sq-CC lens.

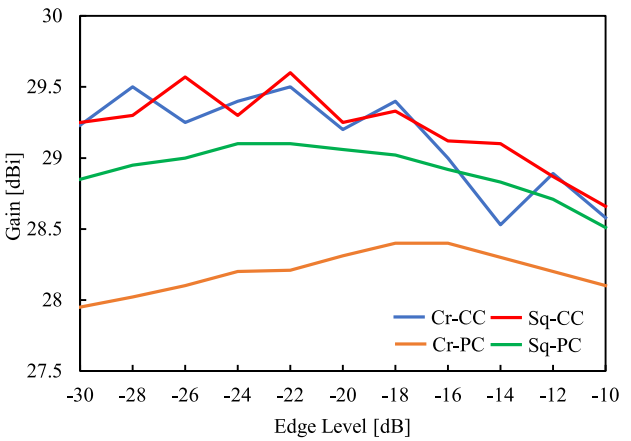

FIGURE 6. Comparison of the gain versus optimized edge level for all four types of lenses at 300 GHz.

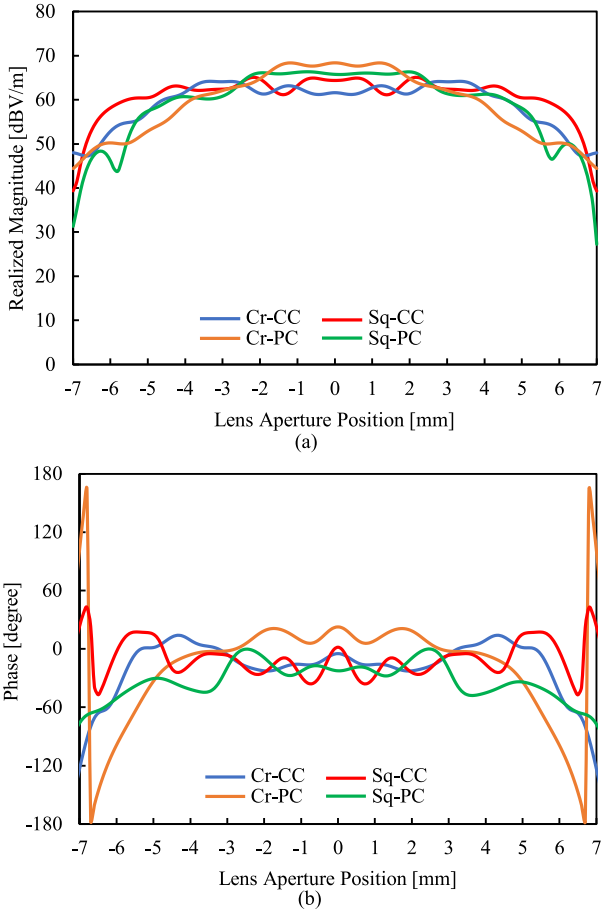

FIGURE 7. Comparison of the aperture (a) amplitude and (b) phase distributions from 1 mm above the lens top at 300 GHz on a diagonally cut plane.

co- efficient, radiation pattern, gain, and antenna efficiency. Fig. 5 shows the side views of the four types of lens shapes: circular plano-convex (Cr-PC), circular concave-convex (Cr-CC), square-bottom plano-convex (Sq-PC), and square-bottom concave-convex (Sq-CC). The dashed lines in Figs. 5 (b) and (d) show the inner curves of the Cr-CC and Sq-CC lenses. The CC lenses are thicker than the PC in term of refracting the rays to the outer path in the lens aperture for a uniform amplitude distribution. The optimum lens edge level influences the gain performance of the lens, which is the balance between the spill over and the aperture distribution.

Fig. 6 shows the gain with respect to the edge level from -10 dB to -30 dB varying m in (8) as discussed in Section II-C. An inherent optimum peak gain can be observed when varying the edge level illuminating the lens from the horn antenna. Considering the majority peak gain obtained by Cr-CC, Sq-PC, and Sq-CC, we used an edge level of -22 dB in the design to obtain the maximum gain of the lens antenna. As the CC design can improve the aperture amplitude distribution, the effect of a larger taper distribution to reduce spillover is more advantageous for increasing the gain. To realize an edge level -22 dB, m was controlled to be 7.63 and the horn aperture dimensions were designed to have a length $l = 1.53$ mm, width $w = 1.1$ mm and height $h = 7$ mm.

In the PC lens design, the gain of the square-bottom lens was approximately 1 dB higher than that of the circular-bottom lens shown in Fig. 6, because the corner areas worked well. On the other hand, the gains in the design of the CC lens were almost the same between the square-bottom lens and the circular-bottom lens because the CC design works fairly well to improve the aperture distribution over the lens. The fluctuations in the gain depending on the edge level were large for the CC design because the lens edge area was effectively exploited by the CC design.

To investigate the uniformity of the aperture distribution on the dielectric lens antennas and confirm the cause of the gain performance, the near-field distribution on a plane 1 mm above the lens top of each single-lens antenna element in the diagonal plane was simulated. The lens areas ranged from -5 to 5 mm and -7 to 7 mm for the circular-bottom lenses and the square-bottom lenses, respectively. The edge level of the primary radiator was commonly -22 dB. Fig. 7 shows a comparison of the aperture distributions along the aperture diagonal plane. Fig. 7 (a) shows the amplitude distributions of the four types of lenses. The aperture distributions

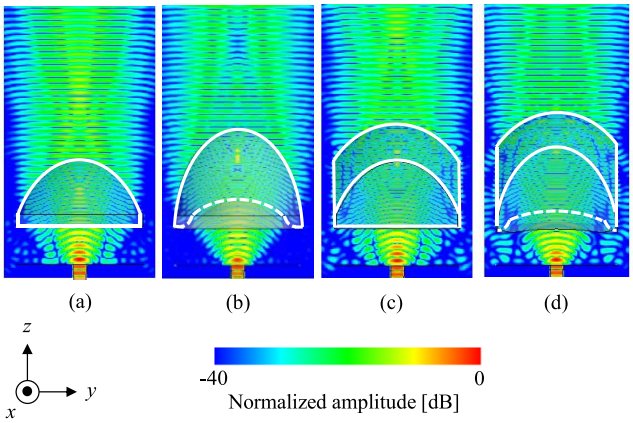

FIGURE 8. Electric-field amplitude distributions in the *yz*-plane (E-plane) including lens axis at 300 GHz (a) Cr-PC lens (b) Cr-CC lens (c) Sq-PC lens, and (d) Sq-CC lens.

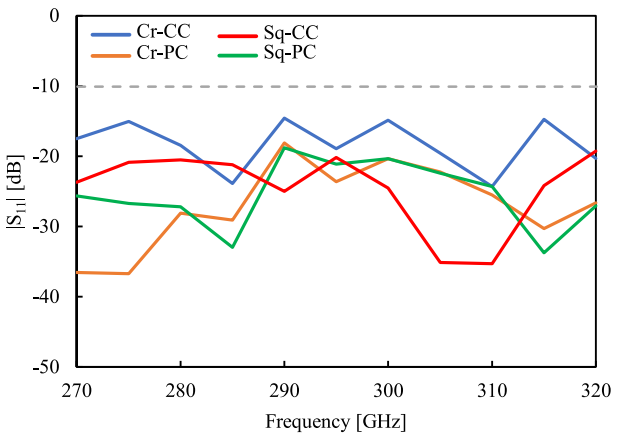

FIGURE 9. Comparison of the reflection coefficient S11 versus frequency for the four types of lenses.

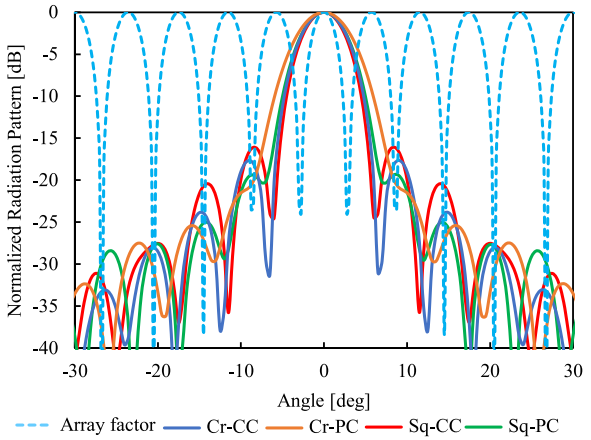

FIGURE 10. Normalized E-plane radiation pattern comparison for the four types of lenses at 300 GHz.

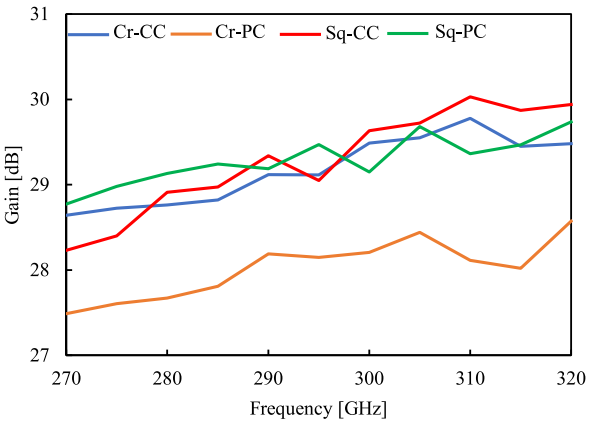

FIGURE 11. Simulated comparison of the gain versus frequency for the four types of lenses in the 300 GHz band.

improved significantly with the CC design for the circular-bottom lens exhibiting a uniform distribution. Therefore, the aperture distribution did not improve from the circular-bottom lens to the square-bottom lens. These facts explain well the gain improvement with the CC design and the square-bottom lens shown in Fig. 6. Fig. 7 (b) shows the phase distributions of the four types of lenses. The phase distributions performed almost uniform in the lens areas.

The electric-field amplitude distributions in the cross sectional *yz*-plane (E-plane), including the lens axis of all four types of lenses, are illustrated in Fig. 8. The CC lens produced a more uniform amplitude distribution than the PC lens. Standing waves are observed in and under the lens. Reflection waves on the outer and inner lens surfaces cause the standing wave distributions. The reflection coefficients of the four types of lens antennas are shown in Fig. 9. The reflection level of the Cr-CC lens is slightly higher than those of the other lenses which may be because the reflected waves at the inner surface back to the horn antenna were emphasized in phase. However, all four types of lens cases are still below -10 dB over a bandwidth of 270-320 GHz.

Fig. 10 shows the normalized radiation patterns in the E-plane for all four single-lens elements. The array factor of the two-element array is overlaid to confirm the possibility of a low SLL in the lens array. The null direction of the lens pattern should coincide with the direction of the grating lobes such that it can be canceled by the null of the array factor, and the first SLL can be reduced. As the Sq-CC lens performs uniform distribution and the beamwidth is narrow, the first nulls are close to the first grating lobes. The radiation pattern of the Sq-CC effectively suppresses the grating lobes of the array factor. On the other hand, the beamwidths of the other lenses are wide; thus, the first sidelobe levels increased. Table 1 presents a simulated comparison of the gain, sidelobe level and half power beam width (HPBW) for all four types of the single-lens elements at 300 GHz. At a design frequency of 300 GHz, the Sq-CC lens showed the highest gain and narrowest HPBW compared to other lenses, whereas the Cr-PC lens exhibited the lowest gain and broadest HPBW.

Fig. 11 shows the gain versus frequency for all four types of lenses in the 300 GHz band including the loss tangent, $\tan\,\delta = 0.001$. The gains increased when the frequency

TABLE 1. Simulated results for single-lens antennas at 300 GHz.

Type of lens	Gain (dBi)	Side-lobe-level, SLL (dB)	HPBW (deg.)
Cr-PC	28.21	−25.42	6.80
Cr-CC	29.48	−17.64	5.62
Sq-PC	29.15	−19.33	5.75
Sq-CC	29.63	−16.10	5.31

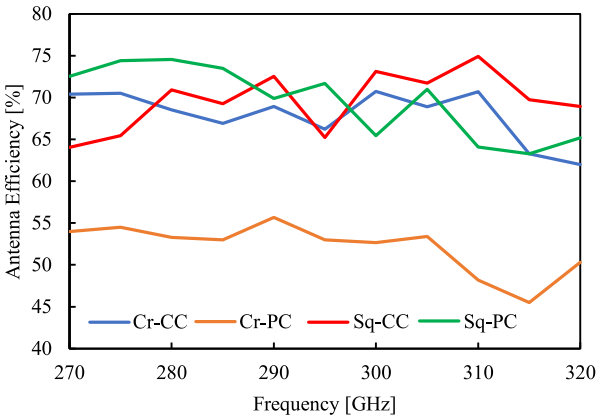

FIGURE 12. Simulated comparison of the antenna efficiency versus frequency for the four types of lenses in the 300GHz band.

increased because the effective aperture area increases with wavelength. The gain of the Sq-CC improved by an average of 1.3 dB compared to a conventional Cr-PC lens. However, the gain differences among the Sq-CC, Cr-CC, and Sq-PC lenses are almost similar in the 300 GHz band.

To investigate the potential of the lens element, the gain and antenna efficiency were evaluated through a simulation. The antenna efficiency η_{eff} is expressed as the ratio of the effective aperture area A_e, to the physical aperture area, A_{phys}, using the following equation:

$$\eta_{eff}(\%) = \frac{A_e}{A_{phys}} \times 100 \tag{10}$$

where the gain G of the aperture plane of the lens antenna is calculated using the effective aperture area, as follows:

$$G = \frac{4\pi}{\lambda^2} A_e \tag{11}$$

where λ is the wavelength of the frequency. The physical aperture area for all four types of lenses was defined as 10 mm × 10 mm, or 100 mm^2. The antenna efficiency versus frequency characteristics for all four types of lenses are shown in Fig. 12. The Sq-CC lens shows the highest average overall efficiency of 65-75% compared to the conventional Cr-PC lens, with approximately 45-55% average overall efficiency throughout the 300 GHz band. In addition, the Sq-PC lens showed an improvement in antenna efficiency compared to the Cr-PC lens. This demonstrates that the rectangular area can be almost fully utilized and helps improve the aperture efficiency using a square-bottom lens.

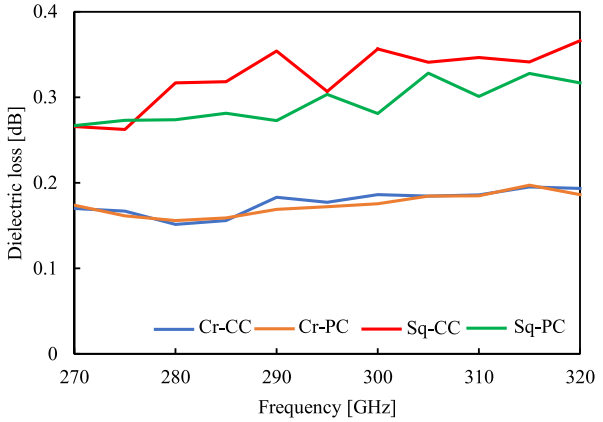

FIGURE 13. Simulated comparison of dielectric loss versus frequency for the four types of lenses in the 300 GHz band.

Therefore, we investigated the conditions based on the effects of dielectric loss and the lens thickness. Fig. 13 shows the dielectric loss versus frequency characteristics for all four types of lenses in the 300 GHz band. We set and divided it into two cases; first, the dielectric loss tangent is set to tan $\delta = 0.001$ and another one to tan $\delta = 0$ for all the frequency bands in all four types of lenses. Therefore, the dielectric loss was determined based on the gain difference between these two cases. The Sq-CC lens exhibited the highest dielectric loss, followed by Sq-PC, Cr-CC, and Cr-PC lenses. The thicker lens contributed to a higher internal loss in the dielectric lens antenna because the distance propagating through the dielectric increased. Therefore, the gain of the Sq-CC lens over the 300 GHz band was limited because of the having a thicker lens. However, square bottom lenses remain higher gain and efficiency by utilizing the entire square aperture.

IV. SIMULATION PERFORMANCE OF LENS ARRAY

This section compares the performance results of a large single lens and the four types of 2 × 2 lens antenna arrays with respect to the radiation pattern, gain, SLL, and antenna efficiency in the 300 GHz band. A large single lens with the same aperture size as the lens array and the same F/D condition was considered and included in this section to compare its overall performance with that of the lens array. The large single lens was designed with a plano-convex (PC) lens shape. The height of the large single lens antenna is 16.50 mm from the aperture of the single horn toward the top of the lens. While the height of the proposed Sq-CC lens antenna is 12.74 mm. Fig. 14 shows the top view geometry of a large single-lens, and the circular and square bottom 2 × 2 lens arrays.

Fig. 15 shows the normalized radiation pattern of the four types of 2 × 2 lens array antennas. To compare their performance, the SLL is an essential parameter to be investigated. Table 2 compares the simulation results of the four types of 2 × 2 lens antennas at 300 GHz. The Sq-CC lens array showed the lowest SLL of −12.5 dB compared

TABLE 2. Simulated results for 2×2 lens array antennas at 300 GHz.

Type of lens	Gain (dBi)	Side-lobe-level, SLL (dB)	HPBW (deg.)
Cr-PC	34.31	−7.65	2.59
Cr-CC	35.47	−10.62	2.51
Sq-PC	35.00	−9.73	2.53
Sq-CC	35.56	−12.50	2.50

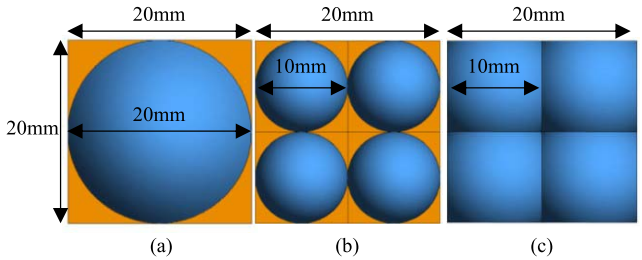

FIGURE 14. Top view of the lens antennas (a) large-single circular-lens, (b) circular-lens array, and (c) square-bottom lens array.

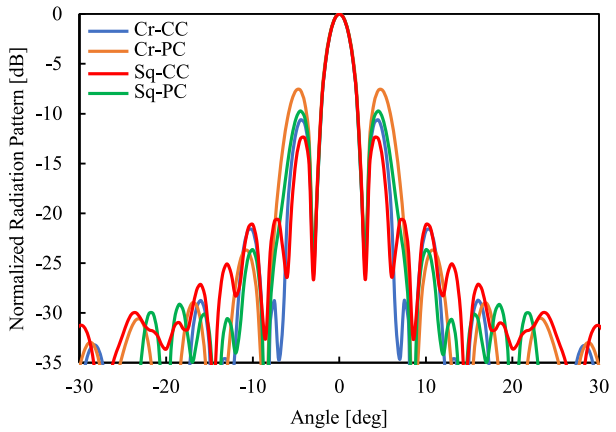

FIGURE 15. Simulated comparison of the normalized radiation pattern for the four types of 2 × 2 lens array antennas at 300 GHz.

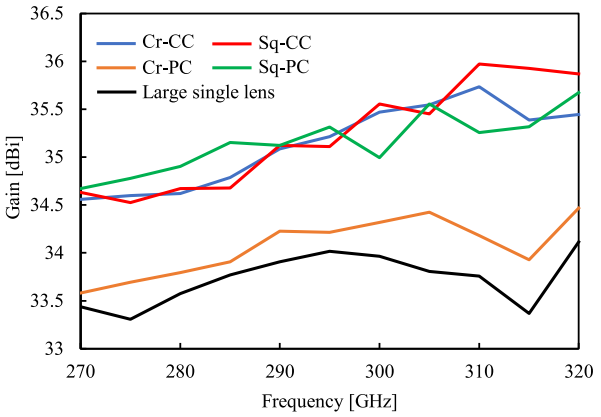

FIGURE 16. Simulated comparison of the gain versus frequency for the four types of lens arrays and a large single lens in the 300 GHz band.

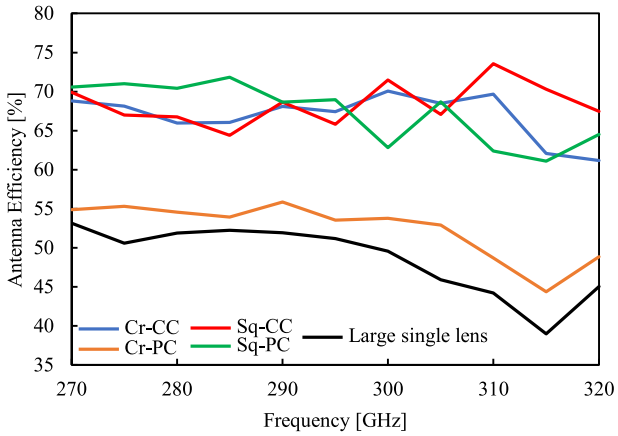

FIGURE 17. Simulated comparison of the antenna efficiency versus frequency for the four types of lens array and a large single lens in the 300GHz band.

to other lens arrays at 300 GHz. The condition of a lower SLL using the Sq-CC lens array confirms that the grating lobes are suppressed by the directive uniform distribution produced by the Sq-CC single lens element patterns (see Fig. 10). This proves that a 2 × 2 lens array Sq-CC lens helps reduce the SLL in the 300 GHz band. At 300 GHz, the conventional Cr-PC lens array provided the high SLL due to insufficient cancellation of grating lobes, as described in Fig. 2. On the other hand, the proposed Sq-CC lens array improves the aperture uniformity and narrows the beamwidth of the lens element. Thus, the grating lobe is suppressed, and the SLL becomes low.

The gain versus frequency characteristics of the four types of the 2 × 2 lens arrays and a large single PC lens is shown in Fig. 16. The Sq-CC lens array shows a consistent gain increase along the bandwidth, which is almost the same trend as that of the single-lens element (see Fig. 11). The proposed Sq-CC lens array enhanced the gain by an average of more than 1.16 dB and 1.5 dB compared with the conventional Cr-PC lens and large single lenses along the bandwidth, respectively. The gain of the large single lens at a design frequency of 300 GHz was 34 dBi. However, the gain differences among Sq-CC, Cr-CC and Sq-PC lenses are almost the same in the 300 GHz band.

Fig. 17 compares the antenna efficiency versus frequency characteristics for all four types of lens arrays and a large single lens in the 300 GHz band. To compare the aperture efficiency, the physical area used in all types of lens antennas was defined as 20 mm × 20 mm or 400 mm^2. As shown in the figure, the trend of the antenna efficiency of the 2 × 2 lens array is almost the same as that of the single-lens element (see Fig. 12). The Sq-CC lens showed the highest average efficiency at the higher frequency side greater than 295 GHz, among other lenses throughout the 300 GHz band. The average overall efficiency of the Sq-CC lens array was approximately 70-75% higher than that of the initially proposed Cr-PC and large single lens over the 300 GHz band. This demonstrates that the rectangular planar array area can be almost fully utilized and helps improve the aperture efficiency using the Sq-CC lens array.

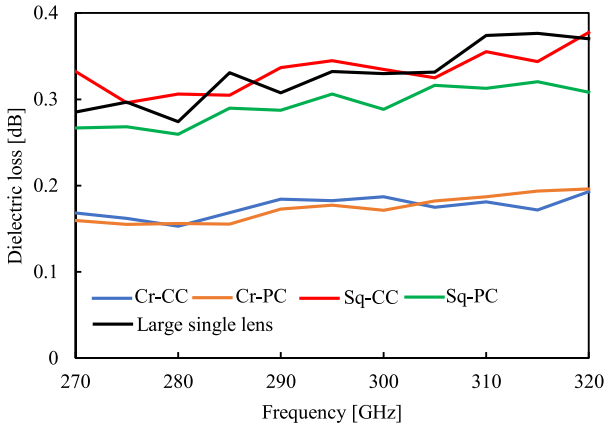

FIGURE 18. Simulated comparison of dielectric loss versus frequency for the four types of lens arrays and a large single lens in the 300 GHz band.

Fig. 18 shows the dielectric loss versus frequency characteristics for all four types of lens arrays and a large single lens in the 300 GHz band. Similar to the results in Fig. 13, the Sq-CC and large single lenses showed the highest dielectric loss, followed by the Sq-PC, Cr-CC, and Cr-PC lenses. The thicker lens contributed to a higher internal loss in the dielectric lens antenna because the distance propagating through the dielectric increased. Therefore, the gain of the Sq-CC lens array over the 300 GHz band was limited because of having a thicker lens. In addition, the large single PC lens also contributed to massive dielectric loss owing to the large diameter of the lens. However, square-bottom lenses remain higher gain and efficiency by utilizing the entire square aperture.

V. EXPERIMENTAL SETUP AND RESULTS

To validate the simulation results of the 2 × 2 lens array and a large single PC lens antenna, we fabricated and measured all the lens antenna prototypes and evaluated their radiation characteristics. The fabricated prototypes of the proposed lens antennas are shown in Fig. 19. All the lens antennas were made of Polypropylene. The lens diameter for all the 2 × 2 lens arrays was 10 mm, whereas that for the large single lens was 20 mm. The lens holder or "jig" was made with the same material as the lens antenna. The jig heights were 3 mm and 6 mm to fix the lens array and the large single lens, respectively. The jig height was based on the F/D ratio of the lens antenna, which was set to 0.3. For the large single lens, the single horn antenna was directly connected to a standard WR-3 feed waveguide. However, the horn array was fed by a four-way power divider into a standard WR-3 feed waveguide for the lens array.

The setup of the near-field measurement system with antenna under test is shown in Fig. 20. The radiation pattern and gain characteristics of the lens antenna were obtained using the XY near-field measurement. Fig. 20 (a) shows the overall setup of the near-field equipment in the chamber room. Fig. 20 (b) shows the antenna probe scanning 2 mm

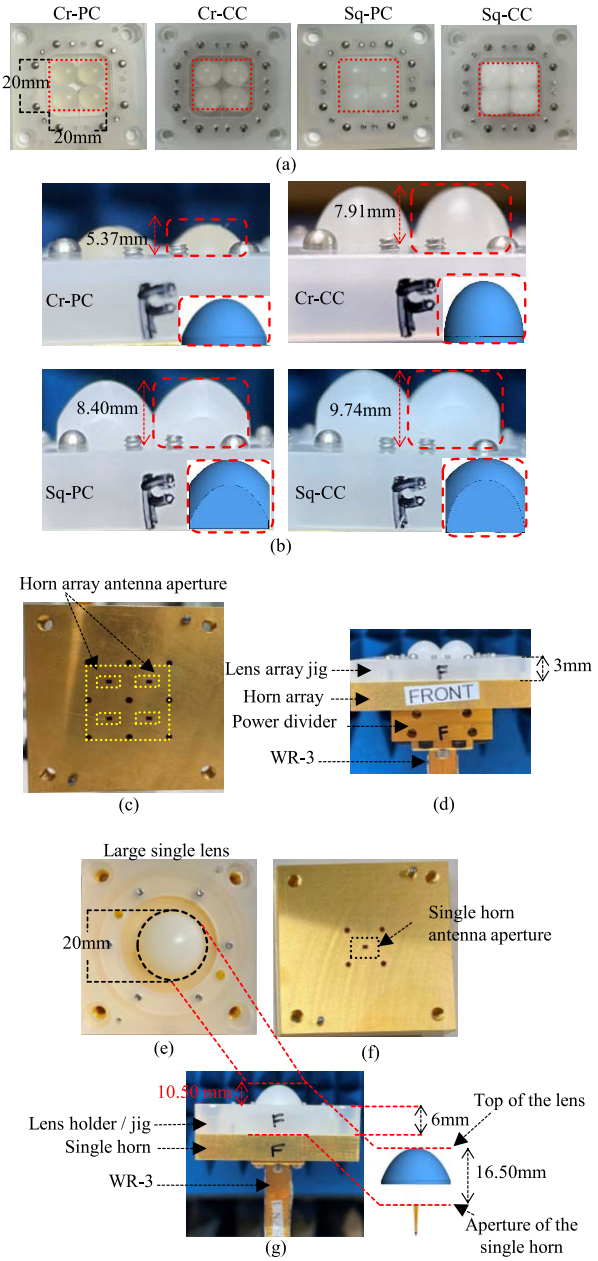

FIGURE 19. Fabricated lenses and primary radiators. (a) Top-view of all the 2 × 2 lens arrays, (b) side-view of all the 2 × 2 lens arrays, (c) top-view of the horn array, (d) side-view of the overall lens array, (e) top-view of large single lens, (f) top-view of the single horn, and (g) side-view of the large single lens antenna.

above the top of the lens AUT and Fig. 20 (c) indicates that the standard gain horn was set at the same position, that is, 2 mm under the probe. The gain was obtained by comparison technique using a standard horn. The sampling pitch and sampling area for the near-field measurement were set to 0.4 mm and 50 mm × 50 mm, respectively at each frequency characteristic from 270 to 320 GHz. A sufficiently wide sampling area was set for measuring the near-field distribution. The size of the measurement area was determined so that the measurement gain was converged with the error smaller than 0.1 dB.

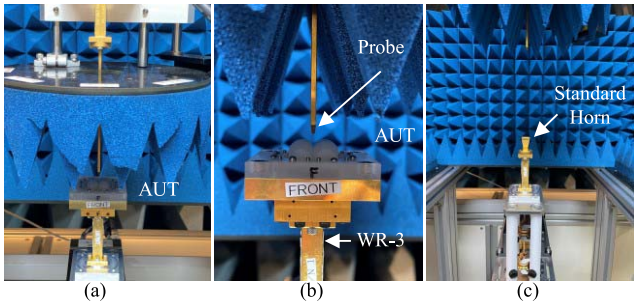

FIGURE 20. Measurement setup for the near-field system (a) overall view, (b) side-view AUT, and (c) side-view standard horn.

TABLE 3. Measured results for 2×2 lens array and large single lens antenna at 300 GHz.

Type of lens	Gain [dBi]	Height of lens in wavelength [λ]	Average gain difference between simulation and measurement [dB]
2 × 2 Cr-PC	32.90	8.4	1.03
2 × 2 Cr-CC	34.83	10.9	0.74
2 × 2 Sq-PC	34.20	11.4	0.75
2 × 2 Sq-CC	34.90	12.7	0.40
Large single PC	32.10	16.5	2.23

Fig. 21 shows a comparison of the simulated and measured normalized E-plane radiation patterns at 300 GHz (left) and the gain versus frequency plots in the 300 GHz band (right) of the 2 × 2 lens array Cr-CC, Cr-PC, Sq-CC, Sq-PC, and a large single lens. Figs. 21 (a) to (d) shows that the measured radiation patterns for all four proposed types of 2 × 2 lens arrays agree almost well with the simulated results. The measured gains for all the 2 × 2 lens arrays were almost the same as those of the simulations. However, some fluctuations were observed between 270 to 320 GHz. There is a gain difference of approximately 0.4 to 1.0 dB in all four types of 2 × 2 lens array antennas. In addition, the 2 × 2 lens array Sq- CC provides the lowest SLL of approximately –12.1 dB compared to other lens arrays owing to a more uniform aperture distribution at the design frequency of 300 GHz.

In Fig. 21 (e), the beamwidth of the measured radiation pattern for the case of a large single lens was broader and the measured gain dropped approximately 2.23 dB over the 300 GHz band compared to the simulated results. We estimated that the differences in the radiation patterns are due to differences in permittivity from the design. The cause of this error should exist in the design of the lens array. The influence of the permittivity error on the radiation pattern became smaller for the lens array since the total radiation pattern is a multiplication of the small single lens pattern and the array factor. However, the effect of the permittivity error appeared much in the radiation pattern of the large single lens. Table 3 provides the measurement comparison

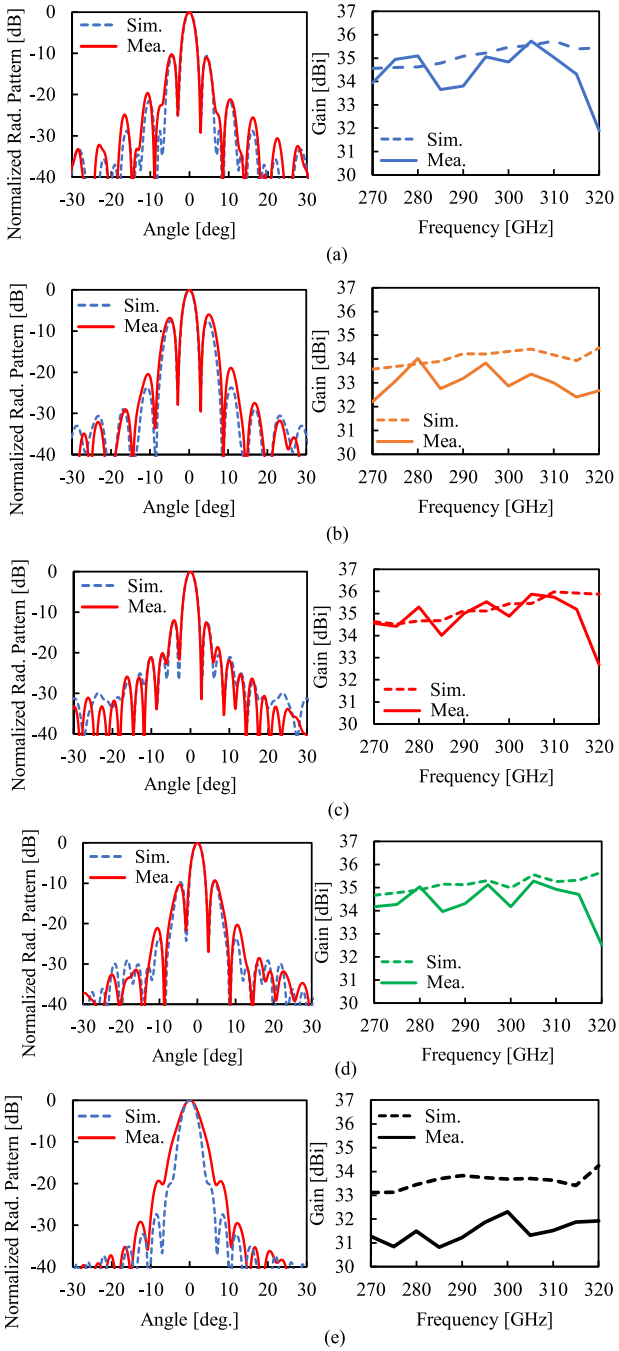

FIGURE 21. Comparison of simulated and measured normalized radiation patterns at 300 GHz (left) and the gain versus frequency plots in the 300 GHz band (right) of the lens array (a) Cr-CC, (b) Cr-PC, (c) Sq-CC, (d) Sq-PC, and (e) large single lens.

results for four types of 2 × 2 lens antenna and a large single lens at 300 GHz. At a design frequency of 300 GHz, the Sq-CC lens array exhibited the highest gain compared to the other lenses, whereas the large single lens exhibited the lowest gain.

Fig. 22 shows the measured antenna efficiency versus frequency characteristics for the 2 × 2 lens arrays Cr-CC, Cr-PC, Sq-CC, Sq-PC, and a large single lens in the 300 GHz band. The value of directivity gain D was obtained from the

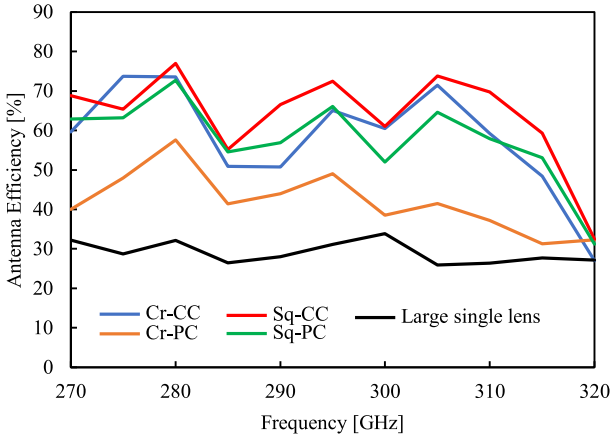

FIGURE 22. Measured overall antenna efficiency versus frequency for the four types of lens array and large single-lens designs in the 300 GHz band.

TABLE 4. Key factor comparison of lens array antennas in this study and prior research.

Ref.	Types of lens	Gain [dBi]	SLL [dB]	Freq. [GHz]	F/D	No. of element
[21]	Extended hemispherical	28.7	N/A	8-20	>3	7
[22]	Half-sphere	16.9	N/A	101	N/A	2 × 2
[23]	Hemi elliptical	37.6-38.8	−10	71-86	1.1	2 × 2
[26]	Elliptical	27	≤ −10	28	N/A	4 × 4
[27]	Elliptical	30	≤ −10	110	N/A	1 × 4
[28]	Elliptical	37.7	<−12	550	1.6	7
This work		**34.9**	**−12.1**	**300**	**0.3**	**2 × 2**

near-field measurement using a comparison technique. To compare the antenna efficiency, the physical aperture area was defined as 20 mm × 20 mm or 400 mm^2. The Sq-CC lens array showed almost the highest efficiency compared to the other lenses, with an average of 70-75% across the wide bandwidth in the 300 GHz band. Table 4 summarizes the key factor comparison of the proposed antenna and selected dielectric lens array antenna designs with various lens shapes and frequencies.

VI. CONCLUSION

The performance of a 2 × 2 lens array composed of Sq-CC shaped lens antennas was presented in this paper. The proposed 2 × 2 lens array with Sq-CC lenses provided an almost uniform aperture distribution, high gain, and low SLL compared with other lenses at the design frequency of 300 GHz. Moreover, the total height of the Sq-CC lens array was lower than that of the large single lens. The sidelobe level of the 2 × 2 lens array composed of the proposed Sq-CC lens antenna elements was reduced by 4.85 dB lower than the lens array composed of the ordinary Cr-PC lens. Then, the gain increased by approximately 2 dB. The proposed lens array technique enables low profile and high gain simultaneously. It can be integrated into the next-generation mm-wave and THz-wave high-performance antenna systems.

REFERENCES

[1] T. S. Rappaport et al., "Wireless communications and applications above 100 GHz: Opportunities and challenges for 6G and beyond," *IEEE Access*, vol. 7, pp. 78729–78757, 2019.
[2] W. Jiang, B. Han, M. A. Habibi, and H. D. Schotten, "The road towards 6G: A comprehensive survey," *IEEE Open J. Commun. Soc.*, vol. 2, pp. 334–366, 2021.
[3] H. J. Song et al., "8 Gbit/s wireless data transmission at 250 GHz," *Electron. Lett.*, vol. 45, no. 22, pp. 1121–1122, 2009.
[4] S. Mumtaz, J. M. Jornet, J. Aulin, W. H. Gerstacker, X. Dong, and B. Ai, "Terahertz communication for vehicular networks," *IEEE Trans. Veh. Technol.*, vol. 66, no. 7, pp. 5617–5625, Jul. 2017.
[5] Y. Takaku, Y. Kaieda, T. Yu, and K. Sakaguchi, "Proof-of-concept of uncompressed 4K video transmission from drone through mmWave," in *Proc. IEEE 17th Annu. Consum. Commun. Netw. Conf. (CCNC)*, 2020, pp. 1–6.
[6] R. Appleby and R. N. Anderton, "Millimeter-wave and submillimeter wave imaging for security and surveillance," *Proc. IEEE*, vol. 95, no. 8, pp. 1683–1690, Aug. 2007.
[7] R. Appleby and H. B. Wallace, "Standoff detection of weapons and contraband in the 100 GHz to 1 THz region," *IEEE Trans. Antennas Propag.*, vol. 55, no. 11, pp. 2944–2956, Nov. 2007.
[8] K. B. Cooper et al., "THz imaging radar for standoff personnel screening," *IEEE Trans. Thz. Sci. Technol.*, vol. 1, no. 1, pp. 169–182, Jan. 2011.
[9] Y. He, Y. Chen, L. Zhang, S. W. Wong, and Z. N. Chen, "An overview of terahertz antennas," *China Commun.*, vol. 17, no. 7, pp. 124–165, 2020.
[10] Y. J. Guo, M. Ansari, R. Ziolkowski, and N. J. G. Fonseca, "Quasi-optical multibeam antenna technologies for B5G and 6G mmWave and THz networks: A review," *IEEE Open J. Antennas Propag.*, vol. 2, pp. 807–830, 2021.
[11] W. Yi, K. Maolong, M. J. Lancaster, and C. Jian, "Micromachined 300-GHz SU-8-based slotted waveguide antenna," *IEEE Antennas Wireless Propag. Lett.*, vol. 10, pp. 573–576, 2011.
[12] J. Xu, Z. N. Chen, and X. Qing, "270-GHz LTCC-integrated high gain cavity-backed fresnel zone plate lens antenna," *IEEE Trans. Antennas Propag.*, vol. 61, no. 4, pp. 1679–1687, Apr. 2013.
[13] T. Tajima, H.-J. Song, K. Ajito, M. Yaita, and N. Kukutsu, "300-GHz step-profiled corrugated horn antennas integrated in LTCC," *IEEE Trans. Antennas Propag.*, vol. 62, no. 11, pp. 5437–5444, Nov. 2014.
[14] K. Konstantinidis et al., "Low-THz dielectric lens antenna with integrated waveguide feed," *IEEE Trans. Thz. Sci. Technol.*, vol. 7, no. 5, pp. 572–581, Sep. 2017.
[15] M. Saleem, M. K. Xie, M. Alkanhal, and M. Saadi, "Effect of dielectric materials on integrated lens antenna for millimeter wave applications," *Microw. Opt. Technol. Lett.*, vol. 61, no. 4, pp. 1079–1083, 2019.
[16] S. Myllymäki, M. Teirikangas, and M. Kokkonen, "$BaSrTiO_3$ ceramic-polymer composite material lens antennas at 220-330 GHz telecommunication applications," *Electron. Lett.*, vol. 56, no. 22, pp. 1165–1167, 2020.
[17] H. Yi, S.-W. Qu, K.-B. Ng, C. H. Chan, and X. Bai, "3-D printed millimeter-wave and terahertz lenses with fixed and frequency scanned beam," *IEEE Trans. Antennas Propag.*, vol. 64, no. 2, pp. 442–449, Feb. 2016.
[18] N. Chudpooti, N. Duangrit, P. Akkaraekthalin, I. D. Robertson, and N. Somjit, "220-320 GHz hemispherical lens antennas using digital light processed photopolymers," *IEEE Access*, vol. 7, pp. 12283–12290, 2019.
[19] R. Ishihara, K. Sakakibara, N. Kikuma, Y. Sugimoto, Y. Yamada, and N. H. A. Rahman, "Measured performance of high gain dielectric lens antenna in 300 GHz band," in *Proc. Int. Symp. Antennas Propag. (ISAP)*, Osaka, Japan, Jan. 2021, pp. 17–18.

[20] B. Baharom et al., "Reduction of surface reflection on dielectric lens antenna by matching periodic square-pillars in 300-GHz band," *IEEE Access*, vol. 11, pp. 8481–8491, 2023.
[21] O. Yurduseven, N. L. Juan, and A. Neto, "A dual-polarized leaky lens antenna for wideband focal plane arrays," *IEEE Trans. Antennas Propag.*, vol. 64, no. 8, pp. 3330–3337, Aug. 2016.
[22] M. Faridani, and B. Ghalamkari, "Four-element lens array antenna for advanced point-to-(multi)point high-bandwidth wireless communication," *J. Comput. Electron.*, vol. 17, pp. 1082–1089, Jul. 2018.
[23] A. Mozharovskiy, A. Artemenko, O. Soykin, and R. Maslennikov, "Lens array antenna for 71-76/81-86 GHz point-to-point applications," in *Proc. 13th Eur. Radar Conf. (EuRAD)*, 2016, pp. 413–416.
[24] B. Baharom, Y. Sugimoto, K. Sakakibara, B. Rohani, N. Kikuma, and Y. Yamada, "Design for uniform aperture distribution of 2×2 lens array using concave-convex lens in THz band," in *Proc. Int. Symp. Antennas Propag. (ISAP)*, Oct./Nov. 2022, pp. 123–124.
[25] H. Zhang, S. Bosma, A. Neto, and N. Llombart, "A dual-polarized 27 dBi scanning lens phased array antenna for 5G point-to-point communications," *IEEE Trans. Antennas Propag.*, vol. 69, no. 9, pp. 5640–5652, Sep. 2021.
[26] S. Bosma, N. Van Rooijen, M. Alonso-Delpino, M. Spirito, and N. Llombart, "First demonstration of dynamic high-gain beam steering with a scanning lens phased array," *IEEE J. Microw.*, vol. 2, no. 3, pp. 419–428, Jul. 2022.
[27] M. Alonso-delPino, S. Bosma, C. Jung-Kubiak, G. Chattopadhyay, and N. Llombart, "Wideband multimode leaky-wave feed for scanning lens-phased array at submillimeter wavelengths," *IEEE Trans. Thz. Sci. Technol.*, vol. 11, no. 2, pp. 205–217, Mar. 2021.
[28] K. A. Shila and G. Mumcu, "A millimeter-wave 2D beam steering antenna using extended hemispherical dielectric lens antenna subarrays," *IEEE Access*, vol. 10, pp. 103065–103073, 2022.
[29] C. A. Balanis, *Antenna Theory: Analysis and Design*, 4th ed. Hoboken, NJ, USA: Wiley-Intersci., 2005, pp. 284–384.
[30] R. C.Johnson, *Antenna Engineering Handbook*. New York, NY, USA: McGraw-Hill, 1993, pp. 2–27.
[31] F. Ansarudin, T. A. Rahman, Y. Yamada, N. H. A. Rahman, and K. Kamardin, "Multi beam dielectric lens antenna for 5G base station," *Sensors*, vol. 20, no. 20, p. 5849, Oct. 2020.
[32] Y. T. Lo and S. Lee, *Antenna Handbook: Volume II, Theory, Applications, and Design, Chapter 16: Lens Antenna*. New York, NY, USA: Springer, 2013, pp. 5–59.
[33] C. J. Sletten, "Chapter 5: Dielectric lens antennas," in *Reflector and Lens Antennas: Analysis and Design Using Personal Computers*. Norwood, MA, USA: Artech House, 1998.
[34] J. Thornton and H. Kao-Cheng, *Modern Lens Antenna for Communications Engineering, Ch. 1.5 Lens Antenna Design*. Hoboken, NJ, USA: Wiley, 2013, pp. 1–48.
[35] A. Mozharovskiy, A. Artemenko, V. Ssorin, R. Maslennikov, and A. Sevastyanov, "High gain millimeter-wave lens antennas with improved aperture efficiency," in *Proc. 9th Eur. Conf. Propag. (EuCAP)*, Lisbon, Portugal, 2015, pp. 1–5.
[36] A. V. Boriskin, R. Sauleau, and A. I. Nosich, "Accurate analysis of the edge taper influence on the performance of hemielliptic lens antennas," in *Proc. 3rd Eur. Conf. Propag. (EuCAP)*, Berlin, Germany, 2009, pp. 3070–3073.

BAZILAH BAHAROM (Graduate Student Member, IEEE) was born in Penang, Malaysia, in 1994. She received the Bachelor of Engineering degree (Hons.) in electronic engineering from Universiti Teknologi MARA, Malaysia, in 2018, and the Master of Science degree in electrical engineering from the Antenna Research Centre, Faculty of Electrical Engineering, Universiti Teknologi MARA in 2020. She is currently pursuing the Ph.D. degree with the Department of Electrical and Mechanical Engineering, Nagoya Institute of Technology, Nagoya, Japan. Her current research interests include dielectric lens antenna and lens array antennas for millimeter-wave applications.

YOSHIKI SUGIMOTO (Member, IEEE) was born in Fukui, Japan. He received the B.Sc. and M.Sc. degrees from the University of Fukui, Fukui, Japan, in 2013 and 2015, respectively, and the Ph.D. degree from Yokohama National University, Yokohama, Japan, in 2018. From 2018 to 2020, he was with Omron Corporation, where he was involved in the development of wireless power transfer systems and millimeter radar signal processing. In 2020, he joined the Nagoya Institute of Technology as an Assistant Professor. His research interests include antenna measurement, scattering problems, and sub-terahertz antenna.

BAKAR ROHANI (Member, IEEE) was born in Malaysia. She received the B.E. degree in communication and computer from Universiti Kebangsaan Malaysia, Malaysia, in 2004, the M.S. degree in telecommunication and information engineering from Universiti Teknologi MARA, Malaysia, in 2012, and the Dr.Eng. degree in physics, electrical and computer from Yokohama National University (YNU), Yokohama, Japan, in 2016. From 2004 to 2012, she was with Hitachi Electronics and Products, Malaysia, as an Engineer in quality analysis and control for Hitachi Media Electronic Japan. From 2016 to 2019, was an Assistant Professor with the Division of Physics, Electrical and Computer Engineering, Graduate School of Engineering, YNU. In 2019, she joined the Millimeter-Wave and Terahertz-Wave Wireless System Laboratory, Nagoya Institute of Technology as a Researcher. Her research interests include MIMO antenna system, array antenna design, channel capacity, characteristic mode analysis, terahertz-wave antenna, and feeding circuits.

KUNIO SAKAKIBARA (Senior Member, IEEE) was born in Aichi, Japan, in 1968. He received the B.S. degree in electrical and computer engineering from the Nagoya Institute of Technology, Nagoya, Japan, in 1991, and the M.S. and D.E. degrees in electrical and electronic engineering from the Tokyo Institute of Technology, Tokyo, Japan, in 1993 and 1996, respectively. From 1996 to 2002, he was with Toyota Central R&D Labs, Inc., Nagakute, where he was involved in the development of antennas for automotive millimeter-wave radar systems. From 2000 to 2001, he was a Guest Researcher with the Department of Microwave Techniques, University of Ulm, Ulm, Germany. In 2002, he joined the Nagoya Institute of Technology as a Lecturer, where he has been an Associate Professor since 2004 and became a Professor in 2012. His current research interests include millimeter-wave antennas and feeding circuits.

NOBUYOSHI KIKUMA (Senior Member, IEEE) was born in Ishikawa, Japan, in 1960. He received the B.S. degree in electronic engineering from the Nagoya Institute of Technology, Japan, in 1982, and the M.S. and Ph.D. degrees in electrical engineering from Kyoto University, Japan, in 1984 and 1987, respectively. From 1987 to 1988, he was a Research Associate with Kyoto University. In 1988, he joined the Nagoya Institute of Technology, where he has been a Professor since 2001. His current research interests include adaptive and signal processing arrays and multipath propagation analysis, mobile and indoor wireless communication, and electromagnetic field theory. He was a recipient of the 4th Telecommunications Advancement Foundation Award in 1989.

YOSHIHIDE YAMADA (Senior Member, IEEE) received the bachelor's and master's degrees in engineering from the Nagoya Institute of Technology, in 1971 and 1973, respectively, and the Ph.D. degree in electrical engineering from the Tokyo Institute of Technology in 1989. He joined the Electrical Communication Laboratories, Nippon Telegraph and Telephone Corporation (NTT) in 1973, and moved to NTT Mobile Communications Network, Inc., (NTT DoCoMo) in 1993. In 1998, he joined National Defense Academy as a Professor. In 2014, he joined the Malaysia Japan International Institute of Technology, Universiti Teknologi Malaysia, Malaysia, as a Professor. His research interests include aperture antennas, array antennas, very small antennas, and radar cross sections. He received the Excellent Paper Award and the Best Tutorial Paper Award from IEICE in 2013 and 2014, respectively. He is a Fellow of the IEICE Japan, a Senior Member of IEEE APS, and a member of ACES.

NURUL HUDA ABD RAHMAN (Member, IEEE) received the M.Eng. degree in electronic from University of Surrey, Guildford, U.K. in 2008, and the Ph.D. degree in electric, electronic and systems engineering from Universiti Kebangsaan Malaysia in 2014. She joined Astronautic Technology (M) Sdn. Bhd., as a Spacecraft Engineer in 2008, where she was involved in various small-class satellite development and research and development projects. In 2014, she joined Universiti Teknologi MARA Malaysia, where she has been working as an Associate Professor. She also received a 2-year Postdoctoral Fellowship under the Malaysia-Japan International Institute of Technology, Universiti Teknologi Malaysia from 2018 to 2019. Her current research interests include antennas for space and terrestrial applications, array antennas, reflector and lens antennas, wearable and flexible antennas, RF and microwave design, and electromagnetic analysis. She has been a Professional Engineer of the Board of Engineers Malaysia since 2019. She has been appointed as the Executive Committee of the IEEE Malaysia AP/MTT/EMC Joint Chapter from 2021 to 2022. She was also the recipient of the Best Professional Paper Award IEEE Malaysia Comsoc & VTS Joint Chapter in 2018 and the Best Paper Award from IEEE Malaysia AP/MTT/EMC Joint Chapter in 2018 and 2019.